Experimental Validation of Methanol Synthesis from Steel Mill Gases Using a Miniplant Setup

Florian Nestler*, Johannes Full, Jan-Marc Jäckle, Johannes Linsenmeier, Johanna Roob, Max J. Hadrich, and Achim Schaadt

DOI: 10.1002/cite.202200022

Supporting Information available online

Utilization of the gas streams generated by the iron- and steel-making industry for the synthesis of synthetic fuels or chemicals is a promising way to kickstart a technical carbon cycle. Methanol synthesis from cleaned blast furnace gas is a challenge for process design and operation due to high inert gas contents and fluctuations in the gas supply. In this work, a miniplant setup with an adiabatic quench bed reactor was operated with cleaned blast furnace gas over a wide range of process conditions. The experimental data obtained were used to validate a simulation model of the miniplant setup with the perspective for an optimization of the process operational parameters. A high agreement between experimental and simulation data could be obtained, validating the applicability of the simulation approach presented in this work.

Keywords: Experimental validation, Methanol synthesis, Power-to-Liquid, Reaction kinetics, Steel mill gases

Received: February 28, 2022; *revised:* April 28, 2022; *accepted:* April 29, 2022

1 Introduction

Methanol synthesis from carbon dioxide (CO_2)-rich gas streams and electrolytically generated hydrogen (H_2) in the context of so-called Power-to-X processes has become a dynamic field of research in the last three decades, as this technology has the potential to mitigate greenhouse gas emissions in both industry and fuel sector [1–3]. Scientific activities are recently focusing on the description of reaction kinetics for synthesis gases (syngases) with high CO_2 contents [4–6], the development of novel catalysts promising higher activities and slower degradation [7–9] as well as the economic assessment of Power-to-Methanol processes [10–13]. On commercial catalysts, methanol synthesis is described by the following two primary reactions:

$$CO + H_2O \rightleftharpoons CO_2 + H_2 \quad \Delta H_R^0 = -41\ \text{kJ mol}^{-1} \tag{1}$$

$$CO_2 + 3H_2 \rightleftharpoons CH_3OH + H_2O \quad \Delta H_R^0 = -50\ \text{kJ mol}^{-1} \tag{2}$$

The hydrogenation of carbon monoxide (CO) was proven in scientific literature to appear via the combination of water-gas-shift (WGS) reaction (Eq. (1)) with subsequent CO_2 hydrogenation (Eq. (2)) rather than via the direct synthesis route [4, 14, 15]. Due to the equilibrium limitation of the reactions, methanol synthesis is usually operated as loop process with unreacted gases recycled [16].

Besides the low fossil feedstock prices for conventional methanol production, the high CO_2 contents in sustainable syngases remain as challenges for sustainable methanol synthesis [17]. The share of CO_2 within the sum of carbon oxides (CO_x) in the syngas is defined by the carbon oxide ratio (*COR*) [3]:

$$COR = \frac{y_{CO_2}}{y_{CO_2} + y_{CO}} \tag{3}$$

While conventional syngases based on gasification of coal or reforming of natural gas are characterized by high CO contents ($COR < 0.5$), sustainable pathways for methanol synthesis typically feature a syngas with *COR* close to 1.0. Among the CO_2 sources currently discussed are gas streams obtained from flue gases, biomass fermentation or direct air capture (DAC) [18]. In this context, gas streams captured from integrated steel mills operated via the blast furnace route can be a viable option to overcome the thermodynamic, kinetic and catalytic limitations caused by high *COR* due to their considerable CO content [3, 19]. In the

Florian Nestler, Johannes Full, Jan-Marc Jäckle, Johannes Linsenmeier, Johanna Roob, Max J. Hadrich, Dr. Achim Schaadt
florian.nestler@ise.fraunhofer.de
Fraunhofer Institute for Solar Energy Systems ISE, Thermochemical Processes, Heidenhofstraße 2, 79110 Freiburg, Germany.

current state of the art, these gases are used to generate internal process heat for the iron- and steelmaking processes. Besides, the gases are also used for the generation of electric power, however, with a very high CO_2 footprint per kWh [20]. Covering approx. 87 % of the gases produced in the coke-oven based steelmaking process, utilization of blast furnace gas (BFG) by a carbon capture and utilization (CCU) process is necessary to achieve a significant reduction of CO_2 emissions in conventional integrated steel mills. However, in comparison to CO_2-based synthesis gas, BFG entails the drawbacks of the requirement for advanced gas cleaning technologies to remove catalyst poisons like sulfur or halogen compounds [21] as well as a high N_2 content of approx. 48 %, which cannot be separated easily from the gas stream due to the presence of CO [22]. The inert gas content y_{inert} in methanol synthesis is determined by the components nitrogen (N_2), methane (CH_4) and argon (Ar) as follows:

$$y_{inert} = \frac{\dot{n}_{CH4} + \dot{n}_{N2} + \dot{n}_{Ar}}{\dot{n}_{tot}} \tag{4}$$

As BFG only contains approx. 4 % H_2, additional H_2 from sustainable sources such as water electrolysis operated using renewable energy is necessary to obtain a syngas suitable for methanol synthesis. As a measure of the H_2 content in the syngas, the stoichiometric number *SN* is defined by Eq. (5):

$$SN = \frac{y_{H2} - y_{CO_2}}{y_{CO_2} + y_{CO}} \tag{5}$$

To avoid side products, $SN > 2.0$ should be kept at the reactor inlet [23]. Once BFG is mixed with additional H_2, the inert gas content of the so-called make-up gas (MUG) fed into the synthesis process decreases depending on the amount of external H_2. Thus, an increase of *SN* would lead towards a decrease in inert gas content and potentially higher reaction kinetics [4]. However, a too high H_2 content can also be detrimental for the reaction kinetics due to the dilution of the carbon oxides in the MUG and loop [4]. Thus, the amount of externally added H_2 to the BFG stream $R_{H2,ext}$ is one important key indicator for the composition of the MUG and is from here on defined as:

$$R_{H2,\,ext} = \frac{\dot{n}_{MUG,H2,ext}}{\dot{n}_{MUG,tot}} \tag{6}$$

In one of our previous publications [3], we showed that BFG-based syngas enriched with external H_2 entails higher inert gas contents compared to conventional state-of-the-art syngas obtained from the natural gas reforming or coal gasification. Thus, alternative process and reactor layouts need to be discussed in the context of the research project Carbon2Chem® to identify economic pathways towards the production of methanol from steel mill gases. Besides the polytropic steam cooled tubular reactor, adiabatic quench reactor layouts with cold syngas fed between the reactor stages for temperature control are widely applied in industry due to their lower investment costs and better capability for scale-up [24]. In order to evaluate the potential of this reactor type for the industrial implementation of methanol synthesis from steel mill gases, an adiabatic quench type miniplant setup is operated by Fraunhofer ISE in the context of the Carbon2Chem® project [25]. In this work, the influence of the process operating conditions on the operation of the miniplant setup will be investigated by an experimental campaign using purified BFG as the CO_x-supplying gas stream. The experimental results will be analyzed and used to validate a process model for methanol synthesis loop processes with adiabatic quench bed reactors.

2 Methods

In order to examine the behavior of methanol synthesis from steel mill gases under realistic conditions, the miniplant setup used throughout this work was installed at the Carbon2Chem® technical center in Duisburg [26]. At this site, the steel mill gases are cleaned, conditioned and supplied to the experimental facilities operated by the project consortium. Thus, fluctuations from the upstream processes at the integrated steel mill and potentially remaining contaminants are passed through to the laboratories to obtain a realistic showcase regarding their influence on process stability in a later scale-up.

Fluctuations in the process parameters and gas composition are known to greatly impact on the performance of methanol synthesis usually implemented as loop process with unreacted syngas recycled to the reactor. In one of our previous works [3], we defined the loop carbon efficiency (*LCE*) and the internal loop hydrogen efficiency (LHE_{int}) as two key performance indicators for assessment of the process quality:

$$LCE[\%] = \frac{\dot{n}_{prod,MeOH}}{\dot{n}_{MUG,CO} + \dot{n}_{MUG,CO2}} \cdot 100\% \tag{7}$$

$$LHE_{int}[\%] = \frac{2\dot{n}_{prod,MeOH} + \dot{n}_{prod,H2O}}{\dot{n}_{MUG,H2}} \cdot 100\% \tag{8}$$

Besides, the performance of the catalyst can be evaluated by the weight time yield (*WTY*) correlating the mass flow of methanol produced to the mass of catalyst in the reactor:

$$WTY = \frac{\dot{n}_{prod,MeOH} M_{MeOH}}{m_{cat}} \tag{9}$$

2.1 Miniplant Setup

The experimental setup used for the validation of the process model during this work is schematically depicted in Fig. 1. The setup was designed, constructed and continuously optimized by Fraunhofer ISE during the

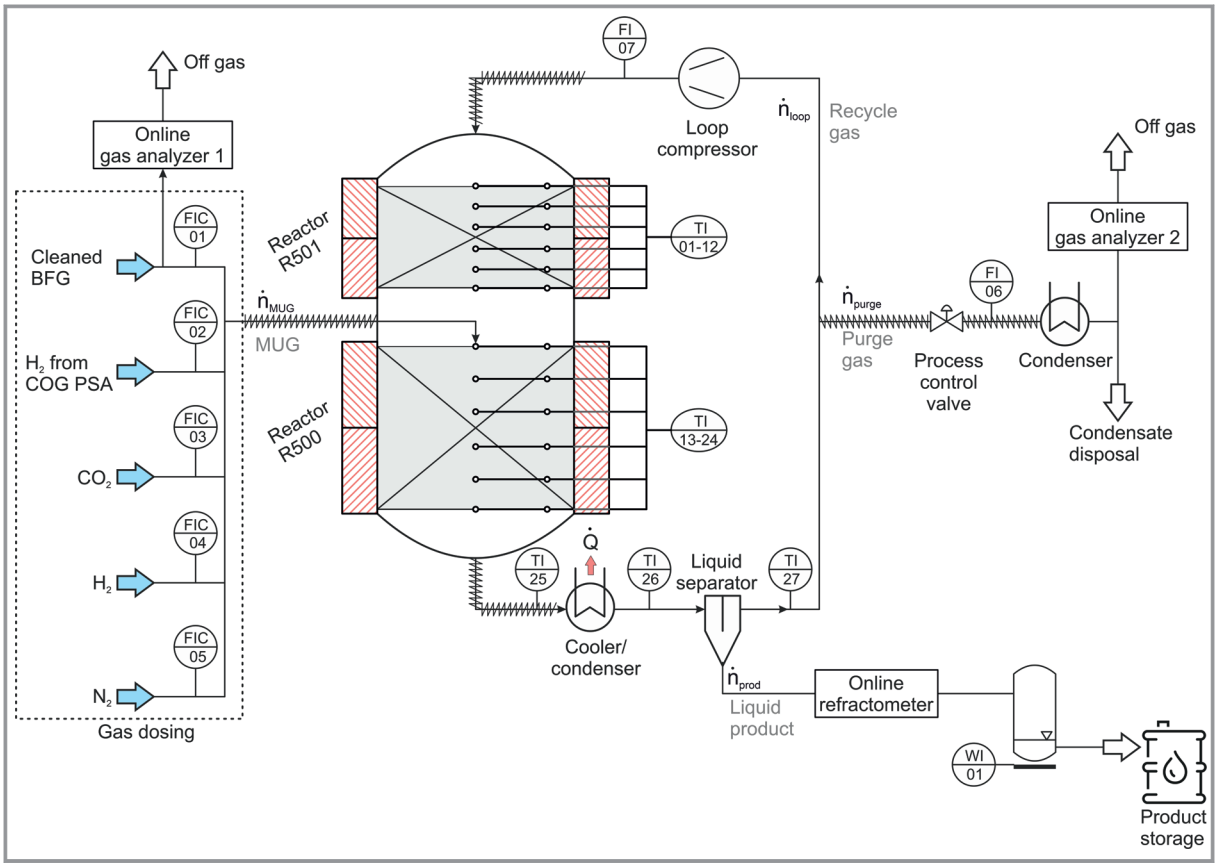

Figure 1. Schematic illustration of the miniplant setup.

Carbon2Chem® project to obtain a plant behavior closely related to an industrial methanol synthesis process [25]. The process layout of the miniplant consists of two adiabatic reactors with the MUG used as a quench gas fed between the reactors, and a recycle loop including a condenser, flash separator, purge gas valve and loop compressor. The miniplant is controlled by remote operation and automated for 24/7 methanol production. For the experimental campaign performed at the technical center in Duisburg, educt gases were preferably dosed from the technical gases supplied on-site from the steel mill gases, i.e., cleaned BFG as well as H_2 obtained from a pressure swing adsorption of coke oven gas via Coriolis flow meters FIC01 and FIC02, respectively. Due to the fluctuating nature of the BFG composition, this stream was permanently analyzed for its main components, i.e., H_2, CO_2, CO, N_2 and CH_4, by an Emerson X-STREAM gas analyzer. Variations in the composition were accounted for by the miniplant control software. Besides the gases produced on site, syngas could also be supplied from gas bottles for CO_2 (FIC03), H_2 (FIC04) and N_2 (FIC05).

The operating pressure of the miniplant setup was set 51 bar absolute pressure for the experiments performed during this study. The gases dosed into the MUG line of the process were heated towards the desired inlet temperature of the reactor R500 and quenched with the product of the loop reactor R501 to reduce the gas temperature and increase the thermodynamic driving force of the reactions. 660 g of full-sized catalyst pellets supplied by Clariant were divided between the two reactors and diluted with α-alumina as inert material. To account for heat losses and the adiabatic temperature increase along the reactors, these were equipped with two-zone heat jackets. In both reactors, the temperatures were monitored by six axially distributed thermocouples in the center and close to the reactor wall, respectively. The temperatures of the heating jackets were adapted to minimize the radial temperature gradient caused by heat losses through the reactor wall along the axial length of the reactors. Further details on the reactor and catalyst particle geometry are provided in Tab. 1.

The liquid products of R500 were condensed with cooling water supplied at temperatures between 15 °C and 20 °C and separated by a cyclone flash separator. The liquid was collected and frequently discharged from the process via a solenoid valve system. Composition of the raw methanol was analyzed by an Abbemat 650 online refractometer. The methanol and water content were determined online by the refractive index according to the methodology presented in [27]. Downstream the refractometer, the liquid product was led into a vessel with a maximum operating pressure of

Table 1. Geometric dimensions of the catalyst beds of the miniplant.

Parameter	Value
d_{in} [m]	0.0635
d_p [m]	0.0054
ρ_{cat} [kg m^{-3}]	1870
$h_{bed,R500}$ [m]	0.322
$h_{bed,R501}$ [m]	0.138
$m_{cat,R500}$ [kg]	0.440
$m_{cat,R501}$ [kg]	0.220

10 bar. The vessel was placed on a balance to determine the amount of liquid product generated. Additional liquid samples were drawn from the mid-pressure vessel periodically and analyzed considering the possible side products. Every time the maximum pressure in the vessel was reached, the product was transferred into a product collection barrel.

The uncondensed gases were recycled to R501 by magnetic-clutch loop compressors. Flow through the compressors was controlled via their shaft rotational speed. The amount of recycle gas was measured using a mass flow meter (FI07) located downstream the loop compressors. The desired recycle ratio *RR* was adapted regarding Eq. (10):

$$RR = \frac{\dot{n}_{loop}}{\dot{n}_{MUG}} \tag{10}$$

The pressure inside the process loop was controlled by a pneumatic pressure regulating valve discharging the purge gas from the process. The mass flow of the purge gas was continuously monitored by a Coriolis flow meter (FI06). Downstream this sensor, the purge gas was dried and fed into a gas analyzer, twin to the BFG analyzer, where the main components H_2, CO_2, CO, N_2 and CH_4 were measured continuously. The complete set of the experimental data was written into a log file with a temporal resolution of 1 s. These data were compressed by creation of overlapping balance intervals with a duration of 60 min starting every 15 min.

2.2 Experimental Campaign

The miniplant setup operated during this experimental study was designed for autonomous 24/7 operation. During the herein discussed experimental campaign, the plant was operated for a time on stream (ToS) of approx. 1340 h. Before the start of the herein described experimental campaign, the catalyst was exposed to synthesis conditions for 1000 h ToS to account for the initial deactivation of the fresh catalyst [17, 28]. To obtain experimental data for the validation of the simulation model, the logged experimental data were filtered to remove outliers and data obtained during non-steady load points. Unusable working points were identified by errors in the C/H/O balances exceeding a value of 5 %. Overall, 1983 balance points were successfully extracted from the raw data.

During the experimental campaign, a set of parameter variations for the process input parameters was carried out for the reactor inlet temperatures, *RR* and $R_{H2,\,ext}$ over the ranges provided in Tab. 2. The flow rate of the MUG was kept constant at $\dot{V}_{MUG}$ = 21 L_N min^{-1}. Unavoidable fluctuations in the BFG composition caused by the steelmaking process were directly passed through to the MUG reflecting the "real-world" challenge of producing chemicals from BFG. Thus, the maximum, minimum and mean values of *SN, COR* and y_{inert} of both the BFG and the MUG are also provided in Tab. 2.

Table 2. Input parameters varied and composition of BFG and MUG obtained during the experimental campaign presented in this work.

Parameter	Min. value	Max. value	Mean value
$T_{in,R500}$ [°C]	171.8	219.8	216.4
$T_{in,R501}$ [°C]	180.7	228.1	225.3
RR [–]	1.0	4.5	4.3
$R_{H2,ext}$ [–]	0.56	0.74	0.65
SN_{BFG} [–]	–0.45	–0.30	–0.37
COR_{BFG} [–]	0.39	0.50	0.46
$y_{inert,BFG}$ [–]	0.43	0.56	0.47
SN_{MUG} [–]	2.14	5.56	3.41
COR_{MUG} [–]	0.39	0.50	0.46
$y_{inert,MUG}$ [–]	0.12	0.22	0.17

During the experimental campaign, the focus was set on the variation of *RR* and $R_{H2,ext}$ as the circulation of the syngas in the loop and the stoichiometry of the gas stream were found important process parameters for the later industrial implementation of the Carbon2Chem® process. To avoid thermal sintering of the catalyst at temperatures exceeding 280 °C due to fluctuations in the syngas composition, the outlet temperature of the two catalyst beds was preferably kept around 260 °C by control of the inlet temperatures of the reactors in order to keep a safety margin [28].

2.3 Simulation Model

2.3.1 Reactors

The simulation of the miniplant process loop was performed using a Matlab© Simulink model. The two reactors were implemented with an ideal adiabatic reactor model applying the following balances for heat, mass and impulse:

$$\frac{dT}{dx} = \frac{\sum \Delta H_{R,i} r_{eff,i} A_R \rho_{bulk}}{c_{p,gas} \dot{n}_{tot}} \quad (11)$$

$$\frac{d\dot{n}_j}{dx} = \rho_{bulk} A_R \sum \upsilon_j r_{eff,i} \quad (12)$$

$$\frac{dp}{dx} = -\left(1.75 + 150 \frac{1-\varepsilon_{bulk}}{Re_p}\right) \frac{1-\varepsilon_{bulk}}{\varepsilon_{bulk}^3 d_p} \rho_{gas} u_0^2 \quad (13)$$

The kinetic model was implemented as Langmuir-Hinshelwood-Hougen-Watson (LHHW) approach according to a previous publication [4]. Further details on the kinetic model are provided in the Supporting Information of this publication. Due to an extrapolation in *COR* below 0.7 and a different catalyst applied in this study, possible disagreements between the simulation and the experimental data were expected [4]. However, as the kinetic model was identified as the most reliable for the catalyst used in this study, it was applied in the simulation without modification.

As full-sized catalyst pellets were utilized in this work, the diffusion limitation had to be considered. Thiele modulus was proven by Lommerts et al. to deliver a good description of the diffusion limitation in methanol synthesis. Thus, this approach was applied throughout this work [4, 29, 30].

2.3.2 Flash Separator

Besides the reactors, the flash separator was one important submodel for the simulation, as the solubility of the gases, predominantly CO_2, greatly affects the composition in the loop process. Experimental data on the vapor-liquid equilibria (VLE) of the components H_2O, MeOH, CO_2, H_2, N_2 and CO available in literature were used to tune the binary interaction coefficients of the equation of state (EoS) by Peng-Robinson (PR) [31] applying the extended standard mixing rule as a temperature-dependent polynomial of 2nd degree as follows:

$$k_{ij} = k_{ij,0} + k_{ij,T} \frac{T}{[K^{-1}]} + k_{ij,T^2} \frac{T^2}{[K^{-2}]} \quad (14)$$

Details on the fitting procedure and the literature data used are provided in the Supporting Information of this work. In Tab. 3, the binary interaction coefficients fitted for the PR EoS using the experimental VLE data are provided are shown. As no experimental VLE data were available for the other binary mixtures relevant for this work, the binary interaction coefficients of zero were assumed for those systems.

Table 3. Temperature dependent binary interaction coefficients obtained from the experimental VLE data for PR EoS.

	$k_{ij,0}$ [–]	$k_{ij,T}$ [K^{-1}]	$k_{ij,T2}$ [K^{-2}]
MeOH-H_2O	0.1789	$-1.435 \cdot 10^{-3}$	$2.011 \cdot 10^{-6}$
CO_2-MeOH	–0.1057	$4.790 \cdot 10^{-4}$	$1.420 \cdot 10^{-7}$
CO_2-H_2O	–0.9317	$4.051 \cdot 10^{-3}$	$-4.489 \cdot 10^{-6}$
CO-MeOH	–0.6376	$1.852 \cdot 10^{-3}$	$-1.247 \cdot 10^{-6}$
H_2-MeOH	–1.5004	$4.309 \cdot 10^{-3}$	$-8.118 \cdot 10^{-7}$
N_2-MeOH	–0.5040	$9.193 \cdot 10^{-4}$	$9.388 \cdot 10^{-7}$

By a detailed analysis of the experimental data, the cyclone flash separator of the miniplant was found to deliver a separation efficiency of approx. 91 %. Thus, this value was used in the simulation model for the experimental validation.

2.4 Validation and Optimization Methodology

For the validation of the simulation model of the miniplant, the balance points obtained from the experimental campaign were clustered consecutively in case of constant process input parameters. A maximum of 10 sequential balance points was clustered into one working point by this approach. Thus, the number of simulations was reduced by factor 9.2 with the result of significant savings in computational time for the validation. After the simulation was executed, the simulation results were allocated to the respective experimental points to determine the deviation between the experimental points and to plot the simulation results. In Fig. 2, the methodology for the selection, clustering and

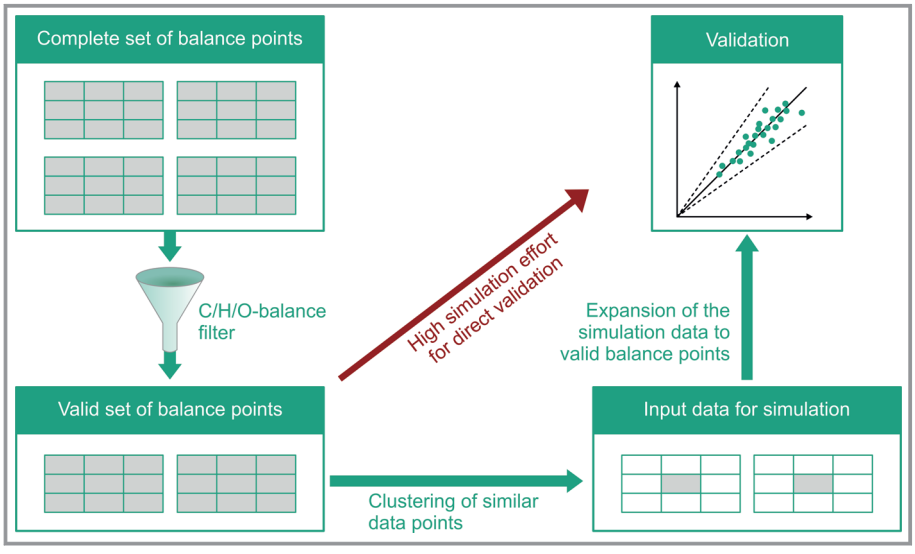

Figure 2. Schematic illustration of the data selection applied for the validation of the simulation model in this work.

validation of the experimental data is provided as schematic diagram of the workflow.

3 Results and Discussion

3.1 Experimental Results

During the experimental campaign presented in this work, fluctuations in the composition of the BFG as noted in Tab. 2, impacted the experimental results. Nonetheless, stable operation of the miniplant was possible and no incidents were caused by fluctuations of the gas compositions. During the experimental campaign, approx. 400 kg of raw methanol were produced from BFG. In Tab. 4, the composition of the process loop gas, the outlet temperatures of the reactors and the key indicators obtained during the experimental campaign are provided.

Table 4. Output parameters obtained from the miniplant during the experimental campaign.

Parameter	Min. value	Max. value	Mean value
SN_{loop} [–]	2.54	29.95	8.02
COR_{loop} [–]	0.50	0.61	0.57
$y_{inert,loop}$ [–]	0.18	0.36	0.29
$T_{out,R500}$ [°C]	249.1	267.2	262.5
$T_{out,R501}$ [°C]	240.4	263.0	259.1
LHE_{int} [–]	22.7	53.3	44.5
LCE [–]	38.3	82.2	70.9

The values for the loop composition clearly indicate the impact of the process loop on the process conditions. While SN_{MUG} reached a maximum value of 5.56 during the experimental campaign (see Tab. 2), H_2 was accumulated in the loop, inducing values of SN_{loop} = 29.95. In a similar manner, inert gases were accumulated in the loop from a mean value of $y_{inert,MUG}$ = 0.17 to $y_{inert,loop}$ = 0.29 during the experimental campaign. Since high inert gas contents in the process loop composition lead towards slower reaction kinetics and lower equilibrium yields, this issue needs to be addressed in a future implementation of an industrial CCU process making methanol from BFG. *COR* in the process loop is influenced by the interaction of WGS reaction (Eq. (1)) and CO_2 hydrogenation (Eq. (2)). While the mean value for COR_{MUG} was 0.46, CO_2 among the carbon oxides was enriched towards a mean value of COR_{loop} = 0.57 during the experimental campaign.

Control of the outlet temperatures of the two reactors turned out to be challenging, as these were sensitive to slight variations in the inlet temperature or fluctuations in gas composition. Moreover, the approach to equilibrium inside R501 impacted the reactions driving force in R500 and consequently the adiabatic temperature rise. However, the critical temperature limit of 280 °C was not exceeded during the experimental campaign.

The high inert gas content in the process loop resulted in high purge gas streams and, therefore, decreased values for LHE_{int} and *LCE*. Maximum values of 53.3 % and 82.2 %, respectively, could be reached within this campaign. Future studies using the validated model to optimize process parameters as the reactor inlet temperatures, *RR*, $R_{H2,ext}$, $\dot{V}_{MUG}$ or the distribution of the catalyst among the two reactor stages will allow to improve the loop efficiencies. Besides, LHE_{int} could be increased further by H_2 recovery from the purge gas, e.g., by membrane technology or pressure swing adsorption [32].

In Fig. 3, a detailed analysis of the variation of $R_{H2,ext}$ is provided by means of MUG composition (A), loop composition (B, C) and reactor outlet temperatures (D). The experimental data were filtered for this analysis to provide similar process working conditions, i.e., RR = 4.5, 0.45 ≤ COR_{MUG} ≤ 0.47, 218 °C ≤ $T_{in,R500}$ ≤ 219 °C and 227 °C ≤ $T_{in,R501}$ ≤ 228 °C. However, slight changes in the reactor inlet temperatures were unavoidable as fluctuations in the syngas composition impacted on the conditions in the loop. As the H-balance error was found to increase at high $R_{H2,ext}$ due to increased analytical inaccuracies, this filter criterion was relaxed from 5 % towards 10 % for this analysis (faded out data points).

Fig. 3A and 3B emphasize the impact of $R_{H2,ext}$ towards the composition in the MUG and loop of the BFG-coupled process. While an increase in SN_{MUG} led towards a lower inert gas content in the loop and potentially better reaction kinetics, surplus in H_2 led towards lower CO and CO_2 partial pressures in the loop with the consequence of slower reaction kinetics. As a consequence, an approach of COR_{loop} to COR_{MUG} was observed with rising $R_{H2,ext}$ (Fig. 3C) representing an activity decrease for the WGS reaction. The negative impact of H_2 accumulation in the loop on the reaction kinetics can also be observed by the outlet temperatures of the two reactors decreasing starting from $R_{H2,ext}$ > 0.65. However, at $R_{H2,ext}$ < 0.60, a decrease in the outlet temperature of R501 can be observed as the consequence of lower catalyst productivity at increasing inert gas contents in the loop. Hence, at the MUG composition obtained from the BFG, a compromise between excess in H_2 and the reduction of the inert gas must be found. This result underlines the importance of $R_{H2,ext}$ for an optimization of BFG-based methanol synthesis processes.

3.2 Validation of the Simulation Model

For the validation of the miniplant simulation model, all data points satisfying the 5% C/H/O-balance criterion were considered. In Fig. 4, the parity plots obtained for the normalized *WTY* (A), SN_{loop} (B), COR_{loop} (C), $y_{inert,loop}$ (D) as well as the outlet temperatures of R500 (E) and R501 (F) are provided.

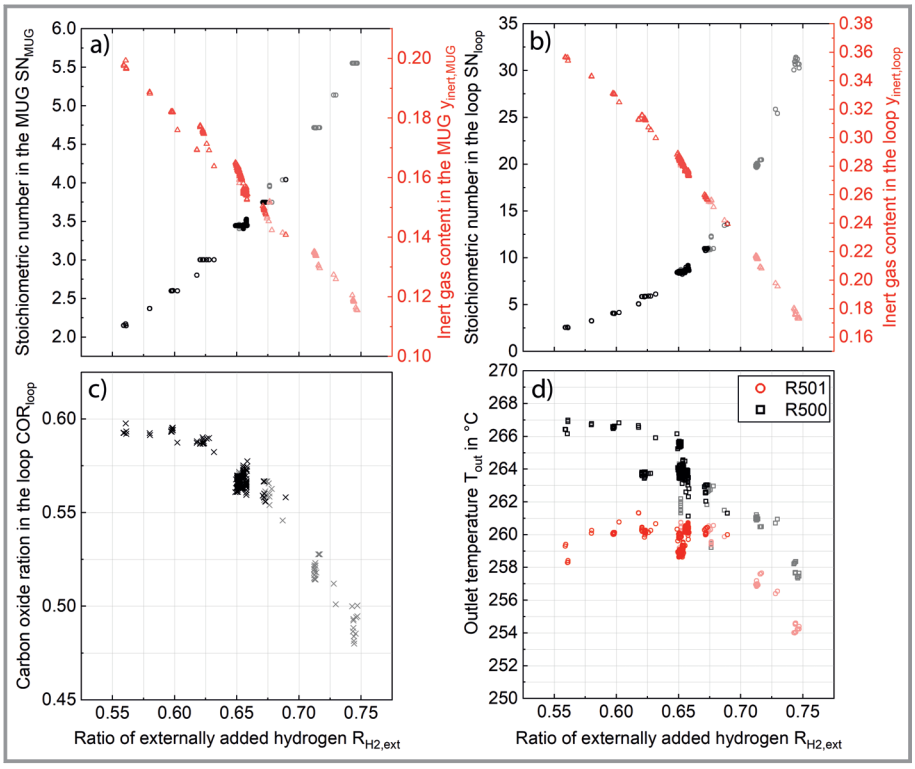

Figure 3. Composition of the MUG by means of SN_{MUG} (a, primary axis) and $y_{inert,MUG}$ (a, secondary axis), composition balancing in the loop regarding to SN_{loop} (b, primary axis), $y_{inert,loop}$ (b, secondary axis), COR_{loop} (c) and outlet temperatures obtained in the two reactors (d) during a variation of $R_{H2,ext}$ between 0.55 and 0.75 at $RR = 4.5$, $0.45 \leq COR_{MUG} \leq 0.47$, $218 \leq T_{in,R500} \leq 219$ and $227 \leq T_{in,R501} \leq 228$; for the faded out data points, the tolerated H-balance error was increased from 5 % towards 10 %.

In the case of the normalized *WTY* (A), all data points simulated for $RR = 4.5$ and $RR = 3.0$ lie within the 10 % error range of the parity plot. This result underlines the high accuracy of the simulation model as 94 % of the experimental points were obtained at these process conditions. However, with a further reduction of *RR*, an increasing systematic deviation between the experimental and simulated data appears in the parity plot. This deviation can probably be explained by lower gas velocities in the reactors and higher axial temperature gradients degrading the plug flow behavior in the catalyst beds. Hence, the operational range of the miniplant should be limited to $RR > 3.0$ in future experimental campaigns used for the validation of the simulation model. Since the highest *WTY* of the miniplant was observed at $RR = 4.5$, the operational points at low *RR* will not be of further interest for future studies using the miniplant setup.

With regard to SN_{loop}, COR_{loop} and $y_{inert,loop}$ in Fig. 4B–D good agreement could be achieved at the operating points with $RR = 4.5$. The slight decrease in model accuracy with increasing SN_{loop} is due to the high sensitivity of this key indicator towards analytical errors in the gas analyzer. In a similar manner to SN_{loop}, model accuracies within the 10 % error range were obtained for $y_{inert,loop}$, however, with the aforementioned tendency of increased deviations at lower recycle ratios. COR_{loop} was underestimated by the simulation model for all data points. While the error remained within the 10 % error range at $RR = 4.5$, increasing inaccuracies were observed with a further reduction of *RR*. As *COR* is highly depending on the interplay of WGS and CO_2 hydrogenation, this finding could be caused by the extrapolation of the kinetic model outside its validated data range ($COR < 0.7$) and the use of a different catalyst [4]. This finding underlines the demand for kinetic measurements at lower *COR* values to obtain a more detailed description of methanol synthesis from steel mill gases.

The parity plots for the outlet temperatures of the reactors R500 and R501 are provided in Fig. 4E and 4F. An agreement within the 10 % error range could be achieved for all data points with $RR \geq 3.0$ indicating the ability of the kinetic model for an appropriate description of the reaction kinetics in this reactor type. The deviations at smaller *RR* are probably caused by the deteriorating plug flow behavior in the reactors at low flow rates mentioned above.

In Fig. 5A, the temperature profiles measured along the reactors are compared for one exemplary working point against their counterparts from the simulation. The graph indicates slight deviations between the measured temperature profiles and the reactor simulations with the tendency of an underestimation of the temperatures as already shown in Fig. 4E and 4F. These differences are most probably caused by a slightly higher activity of the catalyst used in this study and deviations of the miniplant reactors from an ideal adiabatic behavior. However, despite these error influences, the reactor model was highly capable of describing the axial temperature profile along the two reactors.

In order to emphasize the potential of the simulation model for the optimization of the miniplant operation, the approach to equilibrium is depicted in Fig. 5B. For a further increase of the methanol yield, the reactor inlet temperatures of R500 and R501, the amount of quench gas alias $\dot{V}_{MUG}$, and the recycle ratio could be adapted in future work. Moreover, a third reactor stage and/or a redistribution of the catalyst between the stages would enable the miniplant to obtain higher yields. Other than that, allowing higher outlet temperatures and operating pressures would positively affect the productivity. However, the effects of hy-

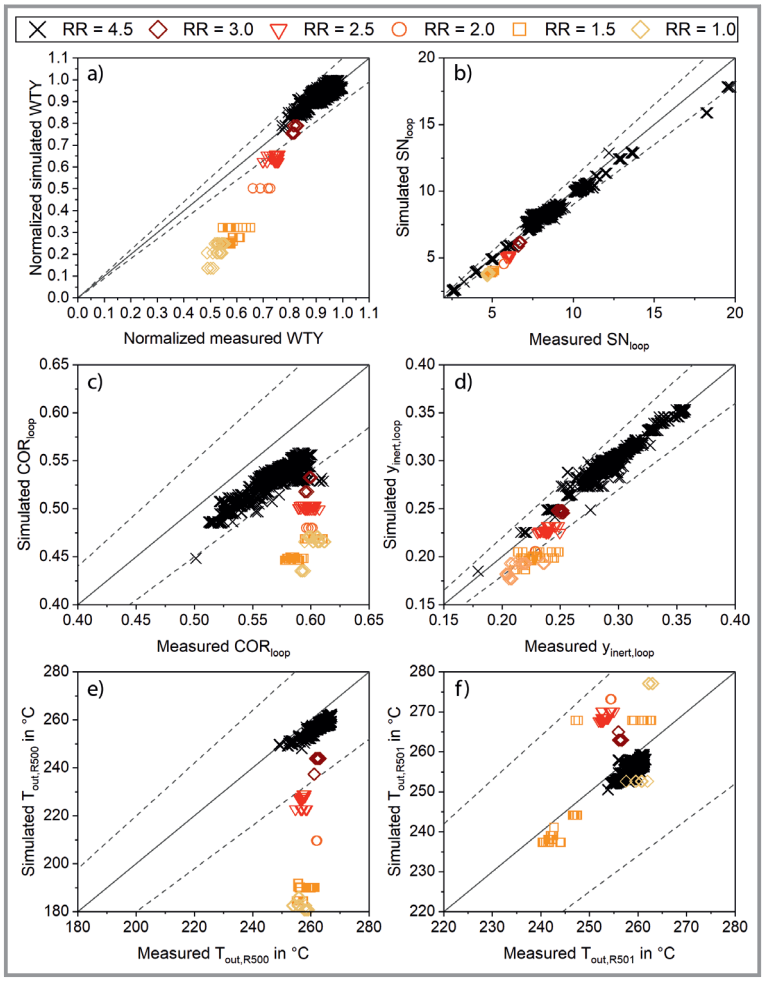

Figure 4. Parity plots of the normalized *WTY* (a), SN_{loop} (b), COR_{loop} (c), $y_{inert,loop}$ (d), $T_{out,R500}$ (e) and $T_{out,R501}$ (f) for all working points considered in this study. Color/symbols indicate the variation in the recycle ratio performed; dashed lines indicate the 10 % error.

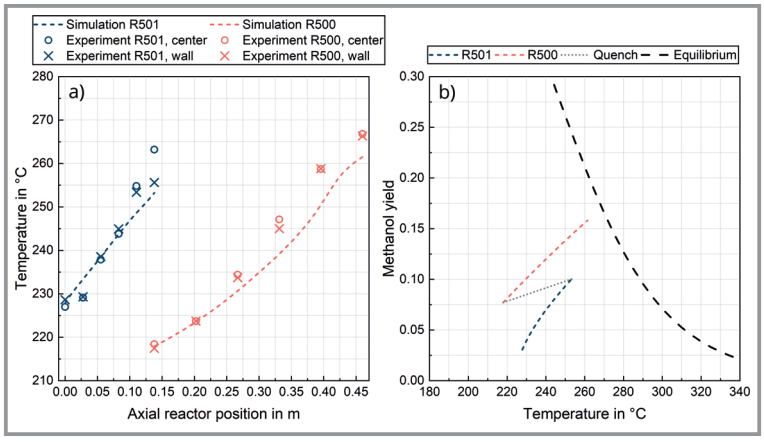

Figure 5. Comparison of the axial temperature profiles obtained from the experiments and the simulation along the reactors (a) and the approach to equilibrium simulated for the gas composition of R500 (b) for a working point at $RR = 4.5$, $R_{H2,ext} = 0.56$, $COR_{MUG} = 0.45$ as well as reactor inlet temperatures of $T_{in,R500} = 217.9\,°C$ and $T_{in,R501} = 227.8\,°C$.

drothermal deactivation of the catalyst at higher temperatures and higher water partial pressures would need to be examined in more detail.

4 Conclusion and Outlook

The experimental results obtained during this study proved that methanol synthesis from real, cleaned BFG can be operated stably over 2300 h ToS without negative consequences for process safety or catalyst activity in a process layout using adiabatic quench bed reactors. Moreover, the complex interplay between the process parameters such as inlet temperatures or SN_{MUG} could be better understood by connecting the experimental results with a process simulation of the miniplant setup. This simulation model was successfully validated as the deviations between experimental and simulation data for the WTY, loop gas compositions and reactor outlet temperatures at the technologically relevant process conditions were less than 10 %. Although the kinetic model used in this study was measured at higher CO_2 contents using a polytropic reactor layout [4], transfer and extrapolation of this model was possible without modifications for the use case described in this work. Finally, these results enable a real-time simulation-assisted optimization of the process operational parameters to increase key indicators such as *WTY*, LHE_{int} or *LCE* of the miniplant under fluctuating process conditions. This optimization is currently being addressed by our group with a promising perspective for further scientific contributions.

Supporting Information

Supporting Information for this article can be found under DOI: 10.1002/cite.202200022. This section includes additional references to primary literature relevant for this research [33–50].

The authors thank the Federal Ministry of Education and Research (Germany) (Bundesministerium für Bildung und Forschung, Verbundvorhaben Carbon2Chem®, support code: 03EW0006F) for funding. Moreover, we would like to dedicate special thanks to the operating team at the technical center in Duisburg for their dedicated and reliable 24/7 support. The catalyst used in this study was kindly provided by project partner Clariant. The project partners of Carbon2Chem® project are kindly acknowledged for their input and contributions to this work. Open access funding enabled and organized by Projekt DEAL.

Symbols used

A_R	[m^2]	cross sectional area
COR	[–]	carbon oxide ratio
c_p	[kJ $mol^{-1}K^{-1}$]	heat capacity
d	[m]	diameter
ΔH_R	[kJ mol^{-1}]	reaction enthalpy
k_{ij}	[–]	binary interaction coefficient
$k_{ij,T}$	[K^{-1}]	binary interaction coefficient, linear T-dependency
$k_{ij,T2}$	[K^{-2}]	binary interaction coefficient, quadratic T-dependency
LCE	[%]	loop carbon efficiency
LHE_{int}	[%]	internal loop hydrogen efficiency
m	[kg]	mass
M	[kg mol^{-1}]	molar mass
$\dot{n}$	[mol s^{-1}]	molar flow
$r_{eff,i}$	[mol $s^{-1}kg_{cat}^{-1}$]	effective reaction velocity
$R_{H2,ext}$	[–]	ratio of externally added H_2
Re	[–]	Reynolds number
RR	[–]	recycle ratio
SN	[–]	stoichiometric number
T	[°C]	temperature
u_0	[m s^{-1}]	empty tube gas velocity
WTY	[g_{MeOH} $kg_{cat}^{-1}h^{-1}$]	weight time yield
x	[m]	axial coordinate
y	[–]	molar fraction

Greek letters

ρ	[kg m^{-3}]	density
ε	[–]	porosity
ν	[–]	stoichiometric factor

Sub- and Superscripts

0	standard conditions
Ar	argon
bed	catalyst bed
cat	catalyst
CH4	methane
CO	carbon monoxide
CO2	carbon dioxide
gas	gas phase
H2	Hydrogen
i	reaction i
in	at inlet / inner
j	component j
bulk	bulk
inert	inert
loop	process loop
MeOH	methanol
MUG	make-up gas
N2	nitrogen
p	particle
purge	purge gas
prod	product
R500	reactor R500
R501	reactor R501
tot	total

Abbreviations

BFG	blast furnace gas
CCU	carbon capture and utilization
CO_x	carbon oxides
DAC	direct air capture
EoS	equation of state
MUG	make-up gas
PR	Peng-Robinson
ToS	time on stream
VLE	vapor liquid equilibrium
WGS	water-gas-shift

References

[1] G. Bozzano, F. Manenti, *Prog. Energy Combust. Sci.* **2016**, *56*, 71–105. DOI: https://doi.org/10.1016/j.pecs.2016.06.001
[2] F. Ausfelder, H. E. Dura, *Optionen für ein nachhaltiges Energiesystem mit Power-to-X Technologien*, 1st ed., DECHEMA Gesellschaft für Chemische Technik und Biotechnologie e.V, Frankfurt am Main **2018**.
[3] F. Nestler, M. Krüger, J. Full, M. J. Hadrich, R. J. White, A. Schaadt, *Chem. Ing. Tech.* **2018**, *90 (10)*, 1409–1418. DOI: https://doi.org/10.1002/cite.201800026
[4] F. Nestler, V. P. Müller, O. Salem, M. Hadrich, A. Schaadt, S. Bajohr, T. Kolb, *React. Chem. Eng.* **2021**, *6*, 1092–1107. DOI: https://doi.org/10.1039/D1RE00071C
[5] F. Nestler, A. R. Schütze, M. Ouda, M. J. Hadrich, A. Schaadt, S. Bajohr, T. Kolb, *Chem. Eng. J.* **2020**, *394*, 124881. DOI: https://doi.org/10.1016/j.cej.2020.124881
[6] S. Ghosh, J. Sebastian, L. Olsson, D. Creaser, *Chem. Eng. J.* **2021**, *416*, 129120. DOI: https://doi.org/10.1016/j.cej.2021.129120
[7] J. Sehested, *J. Catal.* **2019**, *371*, 368–375. DOI: https://doi.org/10.1016/j.jcat.2019.02.002

[8] S. M. Fehr, K. Nguyen, C. Njel, I. Krossing, *ACS Catal.* **2021**, *11 (21)*, 13223–13235. DOI: https://doi.org/10.1021/acscatal.1c03735

[9] I. U. Din, M. S. Shaharun, M. A. Alotaibi, A. I. Alharthi, A. Naeem, *J. CO2 Util.* **2019**, *34*, 20–33. DOI: https://doi.org/10.1016/j.jcou.2019.05.036

[10] F. Schorn, J. L. Breuer, R. C. Samsun, T. Schnorbus, B. Heuser, R. Peters, D. Stolten, *Adv. Appl. Energy* **2021**, 100050. DOI: https://doi.org/10.1016/j.adapen.2021.100050

[11] C. Hank, A. Sternberg, N. Köppel, M. Holst, T. Smolinka, A. Schaadt, C. Hebling, H.-M. Henning, *Sustainable Energy Fuels* **2020**, *4 (5)*, 2256–2273. DOI: https://doi.org/10.1039/D0SE00067A

[12] M. Decker, F. Schorn, R. C. Samsun, R. Peters, D. Stolten, *Appl. Energy* **2019**, *250*, 1099–1109. DOI: https://doi.org/10.1016/j.apenergy.2019.05.085

[13] C. Hank, S. Gelpke, A. Schnabl, R. J. White, J. Full, N. Wiebe, T. Smolinka, A. Schaadt, H.-M. Henning, C. Hebling, *Sustainable Energy Fuels* **2018**, *2 (6)*, 1244–1261. DOI: https://doi.org/10.1039/C8SE00032H

[14] K. G. Chanchlani, *J. Catal.* **1992**, *136 (1)*, 59–75. DOI: https://doi.org/10.1016/0021-9517(92)90106-R

[15] S. Lee, *Methanol synthesis technology*, CRC Press, Boca Raton, FL **1990**.

[16] *Methanol: The basic chemical and energy feedstock of the future: Asinger's vision today* (Ed: M. Bertau), Springer, Berlin **2014**.

[17] F. Pontzen, W. Liebner, V. Gronemann, M. Rothaemel, B. Ahlers, *Catal. Today* **2011**, *171 (1)*, 242–250. DOI: https://doi.org/10.1016/j.cattod.2011.04.049

[18] http://dechema.de/Low_carbon_chemical_industry.html

[19] G. Harp, K. C. Tran, C. Bergins, T. Buddenberg, I. Drach, E. I. Koytsoumpa, O. Sigurbjörnsson, in *METEC & 2nd ESTAD 2015: European Steel Technology and Application Days*, Stahl-Institut VDEh, Düsseldorf **2015**.

[20] G. Harp, in *6th Conference on Carbon Dioxide as Feedstock for Fuels, Chemistry and Polymers*, Cologne, March **2018**.

[21] J. He, D. Laudenschleger, J. Schittkowski, A. Machoke, H. Song, M. Muhler, R. Schlögl, H. Ruland, *Chem. Ing. Tech.* **2020**, *92 (10)*, 1525–1532. DOI: https://doi.org/10.1002/cite.202000045

[22] K. Girod, K. Breitkreuz, T. Hennig, H. Lohmann, S. Kaluza, S. Schluter, *Chem. Eng. Trans.* **2019**, *74*, 475–480. DOI: https://doi.org/10.3303/CET1974080

[23] G. A. Olah, A. Goeppert, G. K. S. Prakash, *Beyond Oil and Gas: The Methanol Economy*, 2nd ed., Wiley-VCH, Weinheim **2009**.

[24] V. Dieterich, A. Buttler, A. Hanel, H. Spliethoff, S. Fendt, *Energy Environ. Sci.* **2020**, *13 (10)*, 3207–3252. DOI: https://doi.org/10.1039/D0EE01187H

[25] M. J. Hadrich, F. Nestler, J. Full, R. J. White, M. Krüger, A. Schaadt, *Chem. Ing. Tech.* **2018**, *90 (9)*, 1137. DOI: https://doi.org/10.1002/cite.201855010

[26] T. Wich, W. Lüke, K. Büker, O. von Morstein, R. Kleinschmidt, M. Oles, R. Achatz, *Chem. Ing. Tech.* **2018**, *90 (10)*, 1369–1374. DOI: https://doi.org/10.1002/cite.201800067

[27] M. Martens, M. J. Hadrich, F. Nestler, M. Ouda, A. Schaadt, *Chem. Ing. Tech.* **2020**, *92 (10)*, 1474–1481. DOI: https://doi.org/10.1002/cite.202000058

[28] M. B. Fichtl, D. Schlereth, N. Jacobsen, I. Kasatkin, J. Schumann, M. Behrens, R. Schlögl, O. Hinrichsen, *Appl. Catal., A* **2015**, *502*, 262–270. DOI: https://doi.org/10.1016/j.apcata.2015.06.014

[29] B. J. Lommerts, G. H. Graaf, A. Beenackers, *Chem. Eng. Sci.* **2000**, *55 (23)*, 5589–5598. DOI: https://doi.org/10.1016/S0009-2509(00)00194-9

[30] J. J. Meyer, P. Tan, A. Apfelbacher, R. Daschner, A. Hornung, *Chem. Eng. Technol.* **2016**, *39 (2)*, 233–245. DOI: https://doi.org/10.1002/ceat.201500084

[31] D.-Y. Peng, D. B. Robinson, *Ind. Eng. Chem. Fund.* **1976**, *15 (1)*, 59–64. DOI: https://doi.org/10.1021/i160057a011

[32] J. M. Bermúdez, A. Arenillas, R. Luque, J. A. Menéndez, *Fuel Process. Technol.* **2013**, *110*, 150–159. DOI: https://doi.org/10.1016/j.fuproc.2012.12.007

[33] G. Soave, *Chem. Eng. Sci.* **1972**, *27 (6)*, 1197–1203. DOI: https://doi.org/10.1016/0009-2509(72)80096-4

[34] M. L. McGlashan, A. G. Williamson, *J. Chem. Eng. Data* **1976**, *21 (2)*, 196–199. DOI: https://doi.org/10.1021/je60069a019

[35] K. Kurihara, T. Minoura, K. Takeda, K. Kojima, *J. Chem. Eng. Data* **1995**, *40 (3)*, 679–684. DOI: https://doi.org/10.1021/je00019a033

[36] P. Sentenac, Y. Bur, E. Rauzy, C. Berro, *J. Chem. Eng. Data* **1998**, *43 (4)*, 592–600. DOI: https://doi.org/10.1021/je970297p

[37] T. Katayama, K. Ohgaki, G. Maekawa, M. Goto, T. Nagano, *J. Chem. Eng. Jpn.* **1975**, *8 (2)*, 89–92. DOI: https://doi.org/10.1252/jcej.8.89

[38] K. Ohgaki, T. Katayama, *J. Chem. Eng. Data* **1976**, *21 (1)*, 53–55. DOI: https://doi.org/10.1021/je60068a015

[39] T. Chang, R. W. Rousseau, *Fluid Phase Equilib.* **1985**, *23 (2–3)*, 243–258. DOI: https://doi.org/10.1016/0378-3812(85)90009-3

[40] E. Brunner, W. Hültenschmidt, G. Schlichthärle, *J. Chem. Thermodyn.* **1987**, *19 (3)*, 273–291. DOI: https://doi.org/10.1016/0021-9614(87)90135-2

[41] K. Suzuki, H. Sue, M. Itou, R. L. Smith, H. Inomata, K. Arai, S. Saito, *J. Chem. Eng. Data* **1990**, *35 (1)*, 63–66. DOI: https://doi.org/10.1021/je00059a020

[42] J. H. Yoon, H. S. Lee, H. Lee, *J. Chem. Eng. Data* **1993**, *38 (1)*, 53–55. DOI: https://doi.org/10.1021/je00009a012

[43] C. J. Chang, C.-Y. Day, C.-M. Ko, K.-L. Chiu, *Fluid Phase Equilib.* **1997**, *131 (1–2)*, 243–258. DOI: https://doi.org/10.1016/S0378-3812(96)03208-6

[44] C. J. Chang, K.-L. Chiu, C.-Y. Day, *J. Supercrit. Fluids* **1998**, *12 (3)*, 223–237. DOI: https://doi.org/10.1016/S0896-8446(98)00076-X

[45] S. N. Joung, C. W. Yoo, H. Y. Shin, S. Y. Kim, K.-P. Yoo, C. S. Lee, W. S. Huh, *Fluid Phase Equilib.* **2001**, *185 (1–2)*, 219–230. DOI: https://doi.org/10.1016/S0378-3812(01)00472-1

[46] R. D'souza, J. R. Patrick, A. S. Teja, *Can. J. Chem. Eng.* **1988**, *66 (2)*, 319–323. DOI: https://doi.org/10.1002/cjce.5450660221

[47] A. Bamberger, G. Sieder, G. Maurer, *J. Supercrit. Fluids* **2000**, *17 (2)*, 97–110. DOI: https://doi.org/10.1016/S0896-8446(99)00054-6

[48] A. Valtz, A. Chapoy, C. Coquelet, P. Paricaud, D. Richon, *Fluid Phase Equilib.* **2004**, *226*, 333–344. DOI: https://doi.org/10.1016/j.fluid.2004.10.013

[49] J. A. Nelder, R. Mead, *Comput. J.* **1965**, *7 (4)*, 308–313. DOI: https://doi.org/10.1093/comjnl/7.4.308

[50] G. H. Graaf, J. G. M. Winkelman, *Ind. Eng. Chem. Res.* **2016**, *55 (20)*, 5854–5864. DOI: https://doi.org/10.1021/acs.iecr.6b00815

